

$E \times B$ flow shear and enhanced confinement in the Madison Symmetric Torus reversed-field pinch*

B. E. Chapman,^{†,a)} A. F. Almagri, J. K. Anderson, C.-S. Chiang, D. Craig, G. Fiksel, N. E. Lanier, S. C. Prager, J. S. Sarff, M. R. Stoneking, and P. W. Terry
Department of Physics, University of Wisconsin-Madison, Madison, Wisconsin 53706

(Received 21 November 1997; accepted 2 February 1998)

Strong $E \times B$ flow shear occurs in the edge of three types of enhanced confinement discharge in the Madison Symmetric Torus [Dexter *et al.*, Fusion Technol. **19**, 131 (1991)] reversed-field pinch. Measurements in standard (low confinement) discharges indicate that global magnetic fluctuations drive particle and energy transport in the plasma core, while electrostatic fluctuations drive particle transport in the plasma edge. This paper explores possible contributions of $E \times B$ flow shear to the reduction of both the magnetic and electrostatic fluctuations and, thus, the improved confinement. In one case, shear in the $E \times B$ flow occurs when the edge plasma is biased. Biased discharges exhibit changes in the edge electrostatic fluctuations and improved particle confinement. In two other cases, the flow shear emerges (1) when auxiliary current is driven in the edge and (2) spontaneously, following sawtooth crashes. Both edge electrostatic and global magnetic fluctuations are reduced in these discharges, and both particle and energy confinement improve. © 1998 American Institute of Physics. [S1070-664X(98)94605-5]

I. INTRODUCTION

The reversed-field pinch is a toroidal magnetically confined plasma configuration distinguished by a toroidal magnetic field whose direction in the plasma edge is opposite that in the core. Confinement of particles and energy in the reversed-field pinch is limited by both electrostatic and magnetic fluctuations, but these fluctuations play different roles in the core and edge (the radius across which the toroidal field reverses is usually taken to be the boundary between the plasma core and edge). According to recent measurements, magnetic fluctuations govern both particle¹ and energy² transport in the plasma core, while electrostatic fluctuations govern particle transport in the edge.³⁻⁵ The mechanism underlying energy transport in the edge has not been established.

In the tokamak, on the other hand, magnetic fluctuations are relatively small, and particle and energy transport are generally believed to be governed everywhere by electrostatic fluctuations. Edge electrostatic fluctuations in some tokamak discharges (referred to as high mode or H-mode discharges) are reduced in the presence of locally sheared $E \times B$ flow.^{6,7} Theoretically,⁸ $E \times B$ flow shear can reduce turbulent fluctuations, and potentially fluctuation induced transport, when the so-called strong shear criterion is satisfied. For $E \times B$ flow to be strongly sheared, the flow shearing rate must be larger than the rate of turbulent radial decorrelation in the absence of flow shear.⁸ In the tokamak, fluctuations are reduced both within and beyond the region of strong shear, leading to a local steepening of the density and/or tempera-

ture profiles and a global improvement in particle and energy confinement.^{6,9}

In all H-mode discharges, the $E \times B$ flow shear emerges due to increased gradients in the radial electric field, induced by a variety of techniques. In one case, these gradients and the associated flow shear are driven by positively or negatively biasing the edge plasma (e.g., see Ref. 10). In another case, the flow shear is generated internally by the plasma when sufficient heat flux passes through the edge plasma.¹¹ This heat flux is sometimes provided by sawtooth crashes, which cause an increase in transport from the core to the edge, but it is more commonly provided by auxiliary (radio frequency and neutral beam) heating.^{6,12-14}

In the Madison Symmetric Torus (MST)¹⁵ reversed-field pinch (RFP), there are three cases where enhanced confinement is accompanied by strong $E \times B$ flow shear. In one case, the plasma edge is positively or negatively biased with insertable probe(s).¹⁶ With sufficient bias, edge floating potential fluctuations are reduced and global particle confinement improves, with little change in energy confinement. In the second case, the $E \times B$ flow shear and enhanced confinement occur spontaneously, following sawtooth crashes.^{17,18} These discharges exhibit a reduction of both the edge electrostatic fluctuations and the core-resonant, global magnetic fluctuations, and both particle and energy confinement improve.

In the third case, the flow shear and enhanced confinement occur with the application of inductive auxiliary current drive (and possibly ohmic heating) in the plasma edge.¹⁹⁻²¹ Again, both electrostatic and magnetic fluctuations are reduced, and both particle and energy confinement improve.¹⁹⁻²¹ The improved confinement in these discharges has been attributed to the reduction of the core-resonant

*Paper kWea11-3 Bull. Am. Phys. Soc. **42**, 1945 (1997).

[†]Invited speaker.

^{a)}Electronic mail: chapman@loki.physics.wisc.edu

magnetic fluctuations brought about by the auxiliary edge current. These fluctuations (tearing modes) are driven by a gradient in the $\mu = \mu_0 \mathbf{J} \cdot \mathbf{B} / B^2$ profile, where \mathbf{J} is the current density, and the purpose of the edge current drive is to reduce this gradient. In this paper, we will discuss the possibility that $\mathbf{E} \times \mathbf{B}$ flow shear can also contribute to the fluctuation reduction in these discharges.¹⁸

Present analytical theory⁸ regarding the reduction of fluctuations by $\mathbf{E} \times \mathbf{B}$ flow shear deals only with short-wavelength electrostatic fluctuations lying entirely within the region of strong shear. This theory can explain some observations of fluctuation reduction in the MST. However, the reduction in the MST includes both long-wavelength electrostatic and global magnetic fluctuations, whose correlation lengths are substantially larger than the width of the shear region. The reduction of long-wavelength electrostatic fluctuations by local flow shear is certainly conceivable, as long as the fluctuations (eddies) overlap the shear region at some location. Further, we will introduce the idea that the flow shear can also affect global magnetic fluctuations (tearing modes), in the case (applicable to the MST) where the flow shear is located well outside the mode's resistive layer or associated islands.²²

II. EXPERIMENTAL APPARATUS AND TECHNIQUE

These experiments were conducted in the MST RFP. The ohmically heated MST plasma has a major radius of 150 cm and a minor radius of 51 cm, determined by graphite limiters covering 10% of the plasma-facing wall. Conditioning of the plasma-facing wall, necessary to a varying degree in all the discharges described here, is accomplished with helium pulsed-discharge cleaning and boronization.²³

Biasing of the plasma edge is accomplished with one or more insertable probes. One type of probe, used thus far for negative bias (electron injection), consists of a miniature plasma source.²⁴ Another type of probe, used for both positive and negative biasing, consists essentially of a biased piece of molybdenum. Typically, from 4 to 8 of the plasma sources are inserted about 4 cm from the plasma boundary to provide the bias (typically $\sim \pm 300$ V) necessary for enhanced particle confinement. Similar results can be achieved with only one of the molybdenum probes, but the probe must be inserted 10–15 cm from the plasma boundary. Unlike the other two types of enhanced confinement discharge, biased discharges are not subject to strict density limits or the need for careful wall conditioning. However, these discharges are limited to relatively low toroidal plasma current (~ 200 – 300 kA) to prevent destruction of the probes.

The discharges with spontaneous confinement improvement, to which we refer henceforth as enhanced confinement (EC) discharges, are achieved subject only to certain operational requirements. The most important are sufficiently low density and sufficiently strong toroidal field reversal, the latter represented by the reversal parameter $F \equiv B_\phi(a) / \langle B_\phi \rangle$, where $B_\phi(a)$ is the toroidal field at the edge, and $\langle B_\phi \rangle$ is the cross-section average. The reversal and density requirements relax with increasing plasma current, I_ϕ . For example, at $I_\phi \sim 200$ kA, the minimum (least negative) $F \sim -0.5$, and the

maximum line-averaged density $\langle n_e \rangle \sim 6 \times 10^{12} \text{ cm}^{-3}$. At 500 kA, the minimum $F \sim -0.2$, and the maximum $\langle n_e \rangle \sim 1.2 \times 10^{13} \text{ cm}^{-3}$. Of the three types of enhanced confinement discharge described in this paper, EC discharges are the most sensitive to the condition of the plasma-facing wall. With poor (contaminated) wall conditions, these discharges are degraded or even prevented altogether. Fueling technique also plays a role in EC discharges, as wall fueling is preferred over gas puff fueling. Wall fueling is achieved by preloading the wall with fuel (hydrogen or deuterium) and turning off the puffing system after initiation of each discharge.

The discharges utilizing auxiliary edge current drive, to which we refer henceforth as pulsed poloidal current drive (or PPCD) discharges, share many of the features of EC discharges (some of which will be shown below). PPCD entails a series of inductively driven edge current pulses whose primary purpose is to tailor the parallel current profile to reduce the global magnetic fluctuations (see Refs. 19–21 for details). These current pulses are brought about by changing the edge toroidal magnetic field, which becomes strongly reversed with PPCD. The best PPCD energy confinement is achieved at relatively low density (e.g., $\langle n_e \rangle \sim 7 \times 10^{12} \text{ cm}^{-3}$ at $I_\phi \sim 200$ kA). The increased reversal of the toroidal magnetic field results in a typical F of ~ -1.0 , but it is not known if this deeper reversal is important to the formation of the strongly sheared flow, as is the case in EC discharges (shown below). PPCD discharges require conditioning of the plasma-facing wall, but they are less sensitive to adverse wall conditions than EC discharges. PPCD discharges also appear to have a dependence on fueling technique similar to that of EC discharges.

Much of the data presented below, including profiles of the plasma potential, floating potential, and ion saturation current, were gathered using Langmuir probes inserted into the edge of MST plasmas. The plasma potential is measured using the swept probe technique, where a sinusoidal bias voltage is applied to the probe tip. Profiles of these electrostatic quantities are mapped out one radial location at a time. In each discharge, data corresponding to periods of improved or standard confinement is time averaged, and time averages from a number of similar discharges are ensemble averaged to arrive at each profile data point. Similarly, fluctuation power spectra result from an ensemble average of spectra measured in a number of similar discharges. All data shown were measured well away from (perturbative) sawtooth crashes.

III. ENHANCED CONFINEMENT AND FLUCTUATION REDUCTION

All three types of enhanced confinement discharge in the MST exhibit improved particle confinement, while only EC and PPCD discharges exhibit improved energy confinement.^{16–21} This is summarized in Table I, which includes standard discharges for comparison. The improved global particle confinement in all three enhanced confinement cases is evidenced by a decreased particle source rate (indicated by neutral hydrogen or deuterium radiation) and a

TABLE I. Energy confinement times and fluctuation behavior for different discharges. Particle confinement improves in all nonstandard cases.

Discharge type	Energy confinement time	Global magnetic fluctuations	Edge electrostatic fluctuations
Standard	1 ms	-----	-----
Biased	1 ms	unaffected	reduced
EC	3 ms	reduced	reduced
PPCD	5 ms	reduced	reduced

line-averaged density that is constant or increasing. The increase in energy confinement time in the EC and PPCD cases occurs with both an increase in the plasma stored energy and a decrease in the ohmic input power.

A. Biased discharges

With the application of bias in the plasma edge, there is a decrease in floating potential fluctuations, which are comprised of fluctuations in the plasma potential and electron temperature. The reduction of floating potential fluctuations, along with the bias-induced change in the plasma potential profile, are illustrated in Fig. 1. These data were gathered in discharges with $I_\phi = 220$ kA and $\langle n_e \rangle \sim 1 \times 10^{13} \text{ cm}^{-3}$. When bias (negative, in this case) is applied to the plasma edge, the plasma potential (V_p) profile steepens substantially, leading to an increased gradient in the radial electric field ($E_r = -\nabla V_p$) profile and increased shear in the $\mathbf{E} \times \mathbf{B}$ flow. This increased shear is reflected by the toroidal flow of impurity ions at different minor radii.¹⁶ At the same time, floating potential fluctuations are reduced over the entire edge, and this reduction is broadband (not shown), spanning the frequency range of the measurement (~ 1 –250 kHz). Thus the reduction includes fluctuations of both large and small spatial scale.

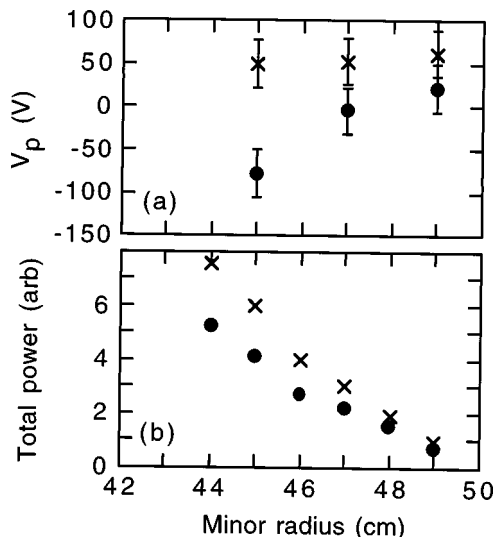


FIG. 1. Profiles of the (a) plasma potential and (b) total fluctuation power (integration over a power spectrum) in the floating potential with (●) and without (×) edge biasing. The biasing probes (plasma sources, in this case) are centered at ~ 46 cm. The plasma boundary is at ~ 51 cm.

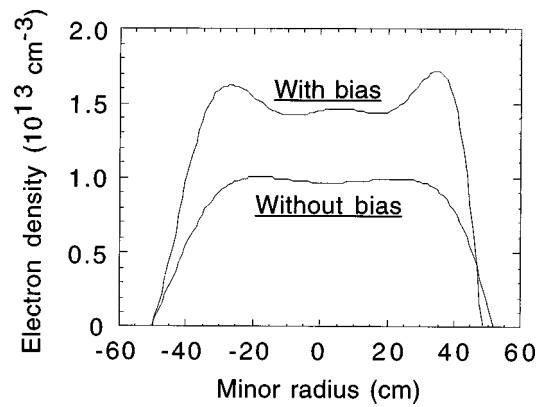


FIG. 2. Electron density profiles with and without edge biasing, measured with an 11-chord interferometer.

In addition to a global improvement in particle confinement with biasing, there is also some evidence for a local improvement in the edge. Shown in Fig. 2 are two electron density profiles in discharges with and without bias. In addition to the difference in total particle number, the profile with bias is substantially steeper in the edge, indicative of locally reduced particle transport.

B. EC discharges

In EC discharges, the improved confinement and increase in edge $\mathbf{E} \times \mathbf{B}$ flow shear occur spontaneously. The plasma potential profiles from standard and EC discharges are shown in Fig. 3. Operationally, these two cases differ only in the reversal of the toroidal magnetic field. $F(\text{EC}) \sim -0.5$, while $F(\text{standard}) \sim -0.2$. The data in Fig. 3, and in the remaining figures in this paper, were recorded at $I_\phi = 200$ kA and $\langle n_e \rangle \sim 5 \times 10^{12} \text{ cm}^{-3}$. The profiles in Fig. 3 illustrate that the change in plasma potential leading to the increase in $\mathbf{E} \times \mathbf{B}$ flow shear occurs locally. The plasma potential changes little from 45 cm out to the plasma boundary.

The reduction of electrostatic and magnetic fluctuations in EC discharges is illustrated in Fig. 4. The floating potential measured 2 cm from the plasma boundary is shown in Fig. 4(a), and in Fig. 4(b) is shown the rms fluctuation in the magnetic field, b_{rms} , measured with an array of magnetic pickup coils at the plasma boundary. Before and after the period of enhanced confinement, fluctuation levels are sub-

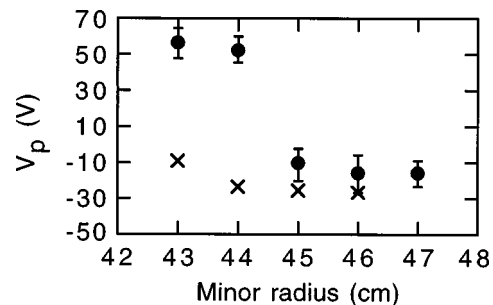


FIG. 3. Profiles of the plasma potential in EC (●) and standard (×) discharges. Error bars for the standard profile (not plotted) are similar to those for the EC profile.

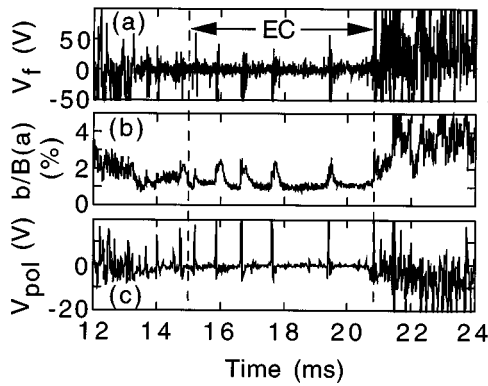


FIG. 4. (a) Floating potential 2 cm from the plasma boundary, (b) rms fluctuation in the magnetic field normalized to the total field at the edge, and (c) surface poloidal voltage during an EC discharge.

stantial, and confinement is degraded. The fluctuation power also increases periodically throughout the EC period. These bursts^{17,18} are manifestations of the RFP dynamo, and they will be described more below.

The dominant contributors to b_{rms} are $m=1$ tearing modes, resonant at various locations in the plasma core. Modes with $m=0$, all resonant at the toroidal field reversal radius (where $q=m/n=0$), also contribute during each dynamo burst. Between bursts, b_{rms} drops to $\sim 1\%$, which is close to the record low $b_{rms} \sim 0.8\%$ achieved during PPCD discharges.²⁰ The $m=1$ modes are driven primarily by gradients in the $\mu = \mu_0 \mathbf{J} \cdot \mathbf{B} / B^2$ profile, and the goal of the PPCD technique is to favorably flatten $\mu(r)$. Thus the reduction of these magnetic fluctuations with PPCD is anticipated. However, their reduction in EC discharges, which utilizes no active current profile control, requires passive profile modification or other explanations.

Shown in Fig. 4(c) is the surface poloidal voltage, which increases in a positive sense with an increase in the toroidal magnetic flux in the plasma volume. The periodic bursts observed during the EC period in the floating potential and b_{rms} also appear in the surface poloidal voltage. Thus they correspond to an increase in toroidal flux, brought about by poloidal current internally generated by the plasma. Such current generation characterizes the RFP dynamo. Another common form of RFP dynamo event is the sawtooth crash,²⁵⁻²⁷ which arises from the rapid destabilization of the core-resonant $m=1$ modes. In contrast to sawtooth crashes, the dynamo events occurring during EC discharges originate with the $m=0$ modes, resonant in the edge.^{17,18,27} The momentary increase in b_{rms} caused by these events is dominantly $m=0$. Note that these events occur during PPCD discharges as well (as will be shown below).²⁸

To further illustrate the reduction of electrostatic fluctuations in EC discharges, we plot standard and EC electrostatic fluctuation power spectra in Fig. 5. As is the case in biased discharges, the fluctuation reduction in EC discharges is broadband ($\sim 1-250$ kHz), including both long- and short-wavelength fluctuations. In the lowermost spectrum in Fig. 5, one observes a local maximum in the fluctuation power at ~ 20 kHz, which is the dominant (rotation) frequency of the

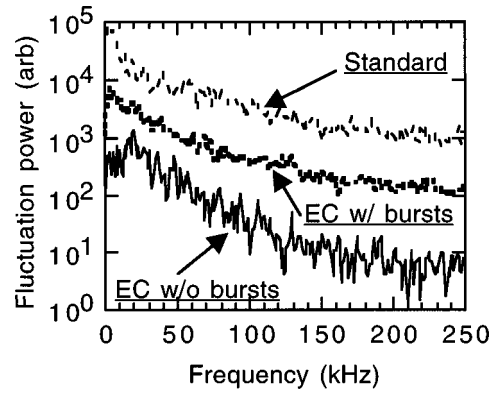


FIG. 5. Fluctuation power spectra calculated from the floating potential 2 cm from the plasma boundary. Two EC spectra are shown, one including and the other excluding the dynamo bursts illustrated in Fig. 4. The lowermost spectrum is noisier than the other two as it is comprised of a smaller ensemble of spectra (four, compared to ~ 25 in the other two).

global $m=1$ tearing modes. The coherence between edge electrostatic (floating potential and ion saturation current) fluctuations and magnetic fluctuations also peaks around 20 kHz.²⁹ Such a correlation is also observed in the edge of the Extrap T1 RFP.³⁰ This may imply that the global magnetic fluctuations drive a low level of electrostatic fluctuations in the edge.

The reduction of electrostatic fluctuations in EC discharges occurs over the entire edge. This is illustrated in Fig. 6(a), in which we plot profiles of the total fluctuation power. Also plotted is the EC plasma potential profile. In addition to the roughly factor of 10 reduction in fluctuation power at all locations, there is an extra reduction in the region of strong $\mathbf{E} \times \mathbf{B}$ flow shear.

As is the case in biased discharges, there is some evidence for an edge reduction of transport in EC discharges, perhaps caused by the $\mathbf{E} \times \mathbf{B}$ flow shear. This is illustrated in

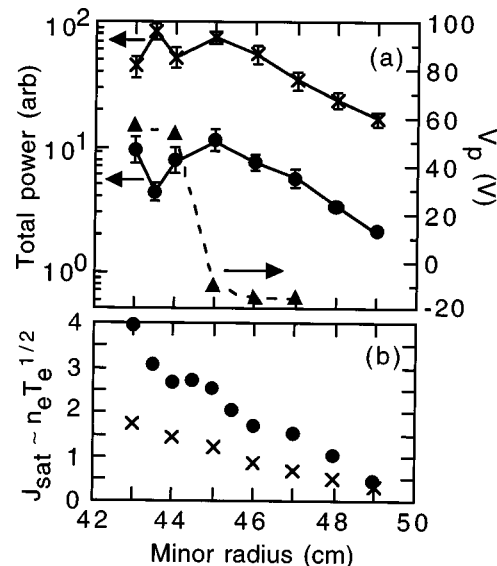


FIG. 6. (a) EC plasma potential profile and EC (\bullet) and standard (\times) profiles of total (integrated) fluctuation power in the floating potential and (b) ion saturation current in both cases. Error bars in (b) are smaller than the plot symbols.

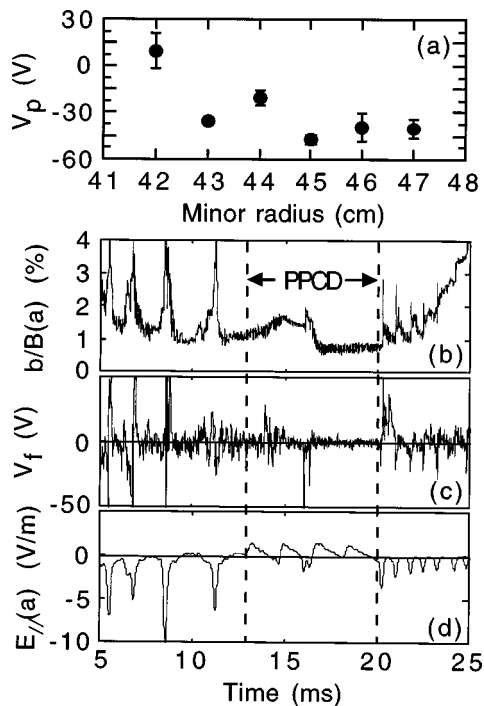


FIG. 7. (a) Plasma potential profile in PPCD discharges, (b) rms fluctuation in the magnetic field normalized to the total field at the edge, (c) floating potential at the plasma boundary, and (d) parallel electric field (calculated from the surface poloidal voltage) at the plasma boundary.

Fig. 6(b), which contains the EC and standard profiles of the ion saturation current, $J_{\text{sat}} \sim n_e T_e^{1/2}$, where T_e is the electron temperature. J_{sat} and ∇J_{sat} are larger over most of the plasma edge in the EC case, implying that ∇n_e and/or ∇T_e are larger. The EC profile is steepest in two locations that overlap the flow shear region, but this profile is flat in the center of the shear region. The increase of ∇n_e and/or ∇T_e in the region of strong shear is consistent with this region acting as a barrier to particle and/or energy transport [the local flattening, where $E_r = -\nabla V_p$ peaks, may result from a minimum in the flow shear].

C. PPCD discharges

Since the core-resonant $m=1$ magnetic fluctuations are driven by a gradient in the parallel current density profile, current profile control has been proposed to reduce these fluctuations. In particular, edge parallel (poloidal) current drive is required in the RFP. PPCD is an inductive, poloidal current drive produced by changing the toroidal magnetic flux, and the reduction of the $m=1$ magnetic fluctuations during PPCD is expected.

Like biased and EC discharges, discharges with PPCD also exhibit increased $\mathbf{E} \times \mathbf{B}$ flow shear in the edge. This is illustrated in Fig. 7(a), which contains the plasma potential profile measured during PPCD discharges. This profile can be compared with the standard profile shown in Fig. 3. The local maximum in the plasma potential at 44 cm (Fig. 7) results in a region of large flow shear broader than that in EC discharges. The reason for this additional structure with PPCD has not been established.

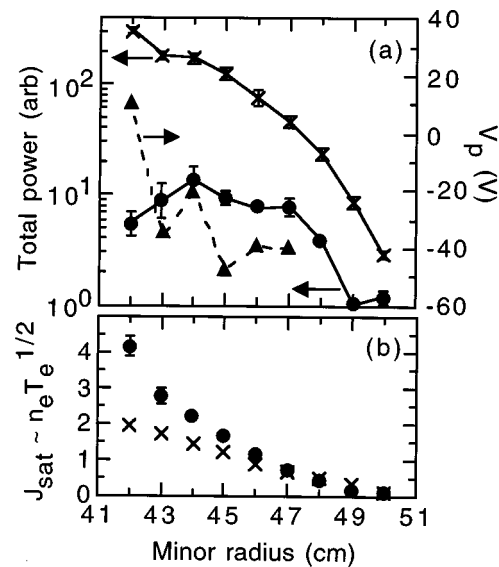


FIG. 8. (a) PPCD plasma potential profile (\blacktriangle) and PPCD (\bullet) and standard (\times) profiles of total (integrated) fluctuation power in the floating potential and (b) ion saturation current in both cases.

Shown in Figs. 7(b)–7(d) is a discharge with PPCD applied. Figure 7(d) depicts the parallel (poloidal) electric field calculated from the surface poloidal voltage. During the PPCD phase of the discharge, one notes four triangular waveforms in the electric field. This illustrates that PPCD in this case is comprised of four individual inductive current pulses. In Figs. 7(b) and 7(c) are plotted the rms fluctuation in the magnetic field and the floating potential at the plasma boundary. In this particular discharge, both magnetic and electrostatic fluctuations decrease in the middle of the PPCD phase. This magnetic fluctuation amplitude is the record-low MST value of 0.8%.²⁰

Also occurring during the PPCD phase are two of the small dynamo bursts, first introduced in Fig. 4. They occur at about 16 ms, just before the fluctuation amplitudes drop. These closely spaced events are most easily observed in the floating potential and parallel electric field, but they also appear in the magnetic fluctuations.

Like biased and EC discharges, the reduction of electrostatic fluctuations during PPCD occurs over the entire plasma edge, and it is broadband (not shown), including fluctuations at low and high frequency. The edge-wide reduction is illustrated in Fig. 8(a), which contains the total electrostatic fluctuation power profiles for PPCD and standard discharges. Also included in this figure is the PPCD plasma potential profile. Where the flow shear is largest, around 43 cm, one observes a local tapering in the fluctuation power, somewhat reminiscent of the fluctuation power profile in the EC case.

There are also indications of a reduction of edge transport during PPCD. The evidence again lies in the ion saturation current profile, presented in Fig. 8(b). The standard profile in this figure is the same as in Fig. 6(b). Compared to the standard case, J_{sat} and ∇J_{sat} are larger from about 46 cm inward with PPCD, implying that ∇n_e and/or ∇T_e are larger. The PPCD profile of J_{sat} is relatively featureless, but one

notes that the profile does steepen with decreasing radius, particularly around 43 cm, where the $\mathbf{E} \times \mathbf{B}$ flow shear is strongest and the total electrostatic fluctuation power is decreasing. Thus the flow shear may be playing a role in the reduction of edge particle and/or energy transport during PPCD.

IV. MECHANISMS FOR FLUCTUATION REDUCTION

A. Electrostatic fluctuations

In biased, EC, and PPCD discharges, electrostatic fluctuations of both large and small spatial scale are reduced within and beyond the region of strong $\mathbf{E} \times \mathbf{B}$ flow shear in the plasma edge. The increased flow shear can play some role in these reductions. Short wavelength fluctuations lying entirely within the region of strong flow shear can be reduced if the strong shear criterion is satisfied.⁸ The flow shear is considered strong if the $\mathbf{E} \times \mathbf{B}$ flow shearing rate is larger than the rate of turbulent radial scattering of fluctuations due to the ambient turbulence (in the absence of $\mathbf{E} \times \mathbf{B}$ flow shear).⁸ For example, in EC discharges, the shearing rate (for the circular RFP) $\omega_s \approx (1/B) \partial E_r / \partial r \sim 7 \times 10^6 / \text{s}$. The turbulence scattering rate is $\sim 3 \times 10^5 / \text{s}$, estimated from the width of the standard-discharge fluctuation power spectrum measured at the radius where the flow shear develops in EC discharges. Thus EC discharges are in the strong shear regime, and fluctuation amplitudes within the shear region are predicted to decrease. This criterion is also satisfied for biased and PPCD discharges.

In addition to the reduction of short wavelength fluctuations, there is also a reduction of long wavelength fluctuations, whose correlation lengths are substantially larger than the width of the flow shear region. To our knowledge, the interaction of such fluctuations with localized $\mathbf{E} \times \mathbf{B}$ flow shear has not been studied analytically. However, as long as a fluctuation (turbulent eddy) overlaps the shear region at some location, one can imagine the shear interrupting "communication" between fluid elements (within the eddy) isolated from one another by the flow shear. This interruption effectively reduces the correlation length of the eddy, which in turn can lead to a reduction in the fluctuation amplitude.⁸

Unlike the previous two cases, the reduction of short-wavelength fluctuations not overlapping the shear region, e.g., those of short wavelength near the plasma boundary, must be explained in some other way (perhaps by a favorable change in some edge gradient).

One additional mechanism for electrostatic fluctuation reduction presents itself, but only for EC and PPCD discharges. In the lowermost power spectrum of Fig. 5, it was shown that the global magnetic fluctuations may drive a low level of electrostatic fluctuations in the edge. Thus the coincident reduction of the magnetic fluctuations in EC and PPCD discharges may contribute to the reduction of the electrostatic fluctuations.

B. Magnetic fluctuations

The global, core-resonant $m=1$ magnetic fluctuations are driven primarily by gradients in the (centrally peaked)

$\mu = \mu_0 \mathbf{J} \cdot \mathbf{B} / B^2$ profile. Thus the reduction of these fluctuations with PPCD is expected, as reduction of $\nabla \mu$ is the purpose of PPCD. However, their reduction in (spontaneous) EC discharges requires either passive μ -profile modification or other explanations. Three nonexclusive possibilities, which may also play a role in PPCD discharges, are based on (1) the reduction of edge resistivity, (2) the small dynamo bursts, and (3) direct interaction with the $\mathbf{E} \times \mathbf{B}$ flow shear.

In the Extrap T1 RFP,³¹ and in simulations,^{31,32} the $m=1$ fluctuation amplitudes are observed to increase (and decrease) with edge resistivity. Measurements of edge resistivity ($\sim Z_{\text{eff}} T_e^{-3/2}$, where Z_{eff} is the mean ionic charge) are not yet available in the MST, but the decreased impurity content and increased bulk temperature of EC and PPCD discharges¹⁷⁻¹⁹ suggest that the resistivity probably decreases.

Each of the small dynamo bursts, first introduced in Fig. 4, is accompanied by a momentary increase in the poloidal (\sim parallel) current in the plasma edge. Thus these bursts may help to reduce $\nabla \mu$ and the $m=1$ magnetic fluctuations. Following the burst of $m=0$ activity associated with each of these events, there is sometimes a decrease (within ~ 0.1 ms) of the $m=1$ mode amplitudes, consistent with a reduction of $\nabla \mu$. However, the $m=1$ amplitudes can sometimes increase in response to these events. Thus the effect of these dynamo bursts varies.

Recent work²² has indicated that it is possible for the flow shear to directly affect the global tearing modes, even though the region of flow shear is located well outside each mode's resistive layer and associated islands. If the flow shear lies within one e -folding length (a toroidal wavelength) of the resistive layer (which is the case in the MST), each mode's growth rate can be reduced when $dV_E/dr > V_A/L_s$, where V_E is the $\mathbf{E} \times \mathbf{B}$ flow velocity, V_A is the Alfvén speed, and L_s is the magnetic shear scale length. This inequality is marginally satisfied for (estimated) MST parameters.

V. CONCLUDING DISCUSSION

To summarize, there are three cases in the MST RFP where enhanced confinement is accompanied by strong $\mathbf{E} \times \mathbf{B}$ flow shear in the plasma edge. Enhanced confinement occurs (1) when the plasma edge is biased, (2) spontaneously, following sawtooth crashes, and (3) when auxiliary poloidal current is driven in the plasma edge. Measurements in standard (low confinement) discharges indicate that global magnetic fluctuations drive particle¹ and energy² transport in the plasma core, while electrostatic fluctuations drive particle transport in the plasma edge.³⁻⁵ In biased discharges, edge electrostatic fluctuations are reduced, and global particle confinement improves. In the other two (EC and PPCD) cases, both edge electrostatic and global magnetic fluctuations decrease, and both the global particle and energy confinement improve.

The $\mathbf{E} \times \mathbf{B}$ flow shear can play a role in the reduction of the electrostatic fluctuations in the edge. It can account for the reduction of short wavelength fluctuations within the shear region and long wavelength fluctuations overlapping

this region. However, it cannot directly affect those fluctuations residing entirely outside the shear region. These fluctuations may be affected by favorable changes in edge gradients or (in the EC and PPCD cases) the coincident reduction of the global magnetic fluctuations.

There are at least three mechanisms which can account for the reduction of magnetic fluctuations in EC and PPCD discharges, in addition to the effect of edge current drive associated with PPCD. These include (1) the reduction of edge resistivity, (2) the dynamo bursts, and (3) direct interaction of the fluctuations with the flow shear. Besides its obvious role in (3), the flow shear may play indirect roles in (1) and (2). By (possibly) reducing particle transport in the edge, the flow shear reduces particle flux to the wall and the resultant impurity influx. This decreases Z_{eff} and can increase T_e , thereby decreasing the edge resistivity. The dynamo bursts are unique to EC and PPCD discharges, and their origin may be tied to the $\mathbf{E} \times \mathbf{B}$ flow shear and its apparent steepening of edge profiles.

Presently, control of the parallel current profile for reduction of global magnetic fluctuations is viewed as the primary path to further improving RFP confinement. However, the possibility now exists that the RFP can also benefit from the effects of $\mathbf{E} \times \mathbf{B}$ flow shear.

ACKNOWLEDGMENTS

The authors are grateful for the assistance of various members of the MST group.

This work was supported by the U.S. Department of Energy. The first author was supported in part by an appointment to the U.S. Department of Energy's Fusion Energy Postdoctoral Research Program administered by the Oak Ridge Institute for Science and Education.

¹M. R. Stoneking, S. A. Hokin, S. C. Prager, G. Fiksel, H. Ji, and D. J. Den Hartog, *Phys. Rev. Lett.* **73**, 549 (1994).

²G. Fiksel, S. C. Prager, W. Shen, and M. R. Stoneking, *Phys. Rev. Lett.* **72**, 1028 (1994).

³T. D. Rempel, C. W. Spragins, S. C. Prager, S. Assadi, D. J. Den Hartog, and S. Hokin, *Phys. Rev. Lett.* **67**, 1438 (1991).

⁴H. Ji, H. Toyama, K. Miyamoto, S. Shinohara, and A. Fujisawa, *Phys. Rev. Lett.* **67**, 62 (1991).

⁵H. Y. W. Tsui, Ch. P. Ritz, G. Miller, J. C. Ingraham, C. P. Munson, K. F. Schoenberg, and P. G. Weber, *Nucl. Fusion* **31**, 2371 (1991).

⁶R. J. Groebner, *Phys. Fluids B* **5**, 2343 (1993).

⁷K. H. Burrell, *Phys. Plasmas* **4**, 1499 (1997).

⁸H. Biglari, P. H. Diamond, and P. W. Terry, *Phys. Fluids B* **2**, 1 (1990).

⁹K. H. Burrell, *Plasma Phys. Controlled Fusion* **36**, A291 (1994).

¹⁰R. J. Taylor, M. L. Brown, B. D. Fried *et al.*, *Phys. Rev. Lett.* **63**, 2365 (1989).

¹¹T. N. Carlstrom, *Plasma Phys. Controlled Fusion* **38**, 1149 (1996).

¹²S. J. Fielding, J. D. Ashall, P. G. Carolan *et al.*, *Plasma Phys. Controlled Fusion* **38**, 1091 (1996).

¹³T. H. Osborne, N. H. Brooks, K. H. Burrell *et al.*, *Nucl. Fusion* **30**, 2023 (1990).

¹⁴Y. Miura, K. Nagashima, K. Itoh *et al.*, *Plasma Phys. Controlled Fusion* **36**, A81 (1994).

¹⁵R. N. Dexter, D. W. Kerst, T. W. Lovell, S. C. Prager, and J. C. Sprott, *Fusion Technol.* **19**, 131 (1991).

¹⁶D. Craig, A. F. Almagri, J. K. Anderson *et al.*, *Phys. Rev. Lett.* **79**, 1865 (1997).

¹⁷B. E. Chapman, C.-S. Chiang, S. C. Prager, J. S. Sarff, and M. R. Stoneking, *Phys. Rev. Lett.* **80**, 2137 (1998).

¹⁸B. E. Chapman, Ph.D. thesis, University of Wisconsin-Madison, Madison, 1997.

¹⁹J. S. Sarff, S. A. Hokin, H. Ji, S. C. Prager, and C. R. Sovinec, *Phys. Rev. Lett.* **72**, 3670 (1994).

²⁰J. S. Sarff, N. E. Lanier, S. C. Prager, and M. R. Stoneking, *Phys. Rev. Lett.* **78**, 62 (1997).

²¹M. R. Stoneking, N. E. Lanier, S. C. Prager, J. S. Sarff, and D. Sinitzyn, *Phys. Plasmas* **4**, 1632 (1997).

²²P. W. Terry, *Bull. Am. Phys. Soc.* **10**, 2047 (1997).

²³D. J. Den Hartog, M. Cekic, G. Fiksel, S. A. Hokin, R. D. Kendrick, S. C. Prager, and M. R. Stoneking, *J. Nucl. Mater.* **200**, 177 (1993); D. J. Den Hartog and R. D. Kendrick, *ibid.* **220-222**, 631 (1995).

²⁴G. Fiksel, A. F. Almagri, D. Craig, M. Iida, S. C. Prager, and J. S. Sarff, *Plasma Sources Sci. Technol.* **5**, 78 (1996).

²⁵J. A. Beckstead, Ph.D. thesis, University of Wisconsin-Madison, Madison, 1990.

²⁶S. Hokin, A. Almagri, S. Assadi *et al.*, *Phys. Fluids B* **3**, 2241 (1991).

²⁷B. E. Chapman, A. F. Almagri, M. Cekic, D. J. Den Hartog, S. C. Prager, and J. S. Sarff, *Phys. Plasmas* **3**, 709 (1996).

²⁸J. S. Sarff, A. F. Almagri, M. Cekic *et al.*, *Phys. Plasmas* **2**, 2440 (1995).

²⁹T. D. Rempel, A. F. Almagri, S. Assadi *et al.*, *Phys. Fluids B* **4**, 2136 (1992).

³⁰G. Li, J. R. Drake, H. Bergsaker *et al.*, *Phys. Plasmas* **2**, 2615 (1995).

³¹P. Nordlund, S. Mazur, H.-E. Satherblom, G. X. Li, J. H. Brzozowski, and J. R. Drake, in *Proceedings of the 15th International Conference on Plasma Physics and Controlled Nuclear Fusion Research, Seville, 1994* (International Atomic Energy Agency, Vienna, 1995), Vol. 2, p. 353.

³²H.-E. Satherblom, S. Mazur, and P. Nordlund, *Plasma Phys. Controlled Fusion* **38**, 2205 (1996).